Korean J. Chem. Eng., 34(7), 2043-2048 (2017)
DOI: 10.1007/s11814-017-0112-3

pISSN: 0256-1115
eISSN: 1975-7220

Quantification of the risk for hydrate formation during cool down in a dispersed oil-water system

Gye-Hoon Kwak*,, Kun-Hong Lee**, Bo Ram Lee*,**,†, and Amadeu K. Sum*,†**

*Hydrates Energy Innovation Laboratory, Department of Chemical & Biological Engineering, Colorado School of Mines, Golden, Colorado, 80401, U.S.A.
**Department of Chemical Engineering, Pohang University of Science & Technology, 77 Cheongam-ro, Nam-gu, Pohang, Gyeongbuk 37673, Korea
(*Received 9 February 2017 • accepted 12 April 2017*)

Abstract−Gas hydrates are considered a nuisance in the flow assurance of oil and gas production since they can block the flowlines, consequently leading to significant losses in production. Hydrate avoidance has been the traditional approach, but recently, hydrate management is gaining acceptance because the practice of hydrate avoidance has become more and more challenging. For better management of hydrate formation, we investigated the risk of hydrate formation based on the subcooling range in which hydrates form by associating low, medium, and high probability of formation for a gas+oil+water system. The results are based on batch experiments which were performed in an autoclave cell using a mixture gas (CH_4 : C_3H_8=91.9 : 8.1 mol%), total liquid volume (200 ml), mineral oil, watercut (30%), and mixing speed (300 rpm). From the measurements of survival curves showing the minimum subcooling required before hydrate can form and hydrate conversion rates for the initial 20 minutes, we developed a risk map for hydrate formation.

Keywords: Gas Hydrates, Flow Assurance, Risk Map, Hydrate Risk Management

INTRODUCTION

Gas hydrates are solid compounds consisting of water as a 'host' and low molecular weight gas as a 'guest' under relatively low temperature and high pressure. The crystalline framework is built from hydrogen-bonded water molecules, forming cages in which gas molecules are trapped within. The structure of gas hydrates is determined by the size and shape of the guest, and the most common are denoted as structure I (sI) and structure II (sII) [1].

One of the areas where gas hydrates are particularly relevant is in the offshore production of oil and gas due to the favorable environment (low temperature, high pressure) for their formation [2]. The formation of hydrates in flowlines is a very serious issue since they can reduce oil and gas production and even form a blockage that stops production and causes hazardous conditions. For these reasons, gas hydrates are a nuisance in the flow assurance of oil and gas production, so there is great interest in controlling/preventing their formation in flowlines [3-9].

Hydrate avoidance (remove production system from hydrate forming conditions) has been the traditional approach used by industry; however, its practice has become more and more challenging due to high costs and operational challenges [10-13]. As such, industry has been looking into hydrate management strategies, that is, control the formation of hydrates and operate the production system understanding the risk posed by hydrates [14]. One of the most critical parts for 'hydrate management' is during transient operations, that is, shut-in and restart operation [15]. During shut-in, fluids in the pipeline are cooled, and depending on the time that the line must be shut-in, preventive measures must be done to prevent hydrate formation upon restart. The conservative approach is to treat the system as soon as hydrate stable conditions are reached. While thermodynamically hydrates are possible to form at the hydrate equilibrium conditions, hydrates often require some degree of subcooling to nucleate and grow.

In this study, we captured the subcooling range in which hydrates have a very low, medium, and high probability of forming by experimentally measuring the conditions for a gas+oil+water system. We performed batch experiments in an autoclave cell. In all experiments, the gas (CH_4 : C_3H_8=91.9 : 8.1 mol%), total liquid volume, mineral oil, watercut (30%), and mixing rate (300 rpm) were fixed. In the first type of experiments, the system was saturated at different pressures (6.9, 10.3 and 13.8 MPa), then cooled down to 277.15 K at a constant cooling rate (4 K/hr or 6 K/hr) from room temperature. The subcooling at which hydrates formed was determined from temperature increase by exothermic reaction, pressure drop by gas trapped, and visual observation through the windows of the cell. These results were analyzed in terms of survival curves, showing that there is i) a minimum subcooling required before hydrate can form, ii) a range of subcooling with a distribution of hydrate formation, and iii) a threshold subcooling for which hydrates will always form. In separate experiments, the hydrate growth rate was measured for different sets of temperature and pressure conditions. To-

†To whom correspondence should be addressed.
E-mail: asum@mines.edu, boramlee.hydrates@gmail.com
‡This article is dedicated to Prof. Ki-Pung Yoo on the occasion of his retirement from Sogang University.

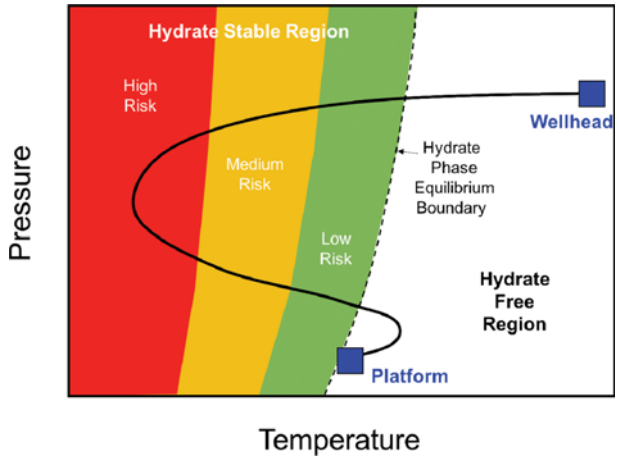

Fig. 1. Illustration of the risk map for hydrate formation in oil and gas production.

gether with the subcooling data, the results were combined to develop a risk map for hydrate formation considering regions of low, medium and high probability, as illustrated in Fig. 1. Fig. 1 also illustrates how the concept of the presented results could be used in determining the regions of a production system likely to have hydrate formation.

EXPERIMENTAL

Fig. 2 shows a schematic of the experimental system used in this study. The pressure cell (inner volume: 270 ml) is made of stainless steel and designed for pressures up to 20 MPa. Two round windows (3 cm in diameter) made of tempered glass are positioned at the front and back of the cell, which makes visual observation for hydrate formation possible with a camera system. An anchor type impeller coupled with a magnetic drive system mixes the contents of the cell. For all experiments, deionized water (dyed in pink), mineral oil 70T (specific gravity: 0.825 at 298 K, viscosity: 21 cP at 293 K, dyed blue), and gas (CH_4 : C_3H_8=91.9 : 8.1 mol%, General Air) were used in this study. Two T-type thermocouples (±1.0 K) monitored each temperature of gas and liquid phase, and a pressure transducer (WIKA, S-20, uncertainty: 0.125%) monitors the system pressure. All data were recorded by a data acquisition system in the computer. A one liter vessel was connected with pressure cell, which was used to increase the gas phase volume; since the system is constant volume, the pressure decrease was relatively small compared to the amount of gas consumed due to hydrate formation, allowing the system to remain nearly at constant pressure. The cell was immersed in a temperature-controlled bath connected to a refrigerated/heating circulator containing ethylene glycol and water mixture. A total of 200 ml liquid of water/oil mixture was used for the tests; with this liquid volume, the impeller was nearly completely submersed, providing consistent and uniform mixing, as shown in Fig. 2. To determine the appropriate mixing speed for the impeller, many visual tests (see Supporting Information) were performed. For the reported measurements, 300 rpm was selected, corresponding to a rotational speed that provided enough mixing to form a water/oil dispersion.

To quantify the risk of hydrate formation, two experimental methods were used, as shown in Fig. 3: (a) subcooling measurements with a constant cooling rate (4 K/hr or 6 K/hr), and (b) formation rate measurements at a specific temperature and pressure. For the subcooling measurements (Fig. 3(a)), 200 ml of liquid sample containing 30% watercut (60 ml water+140 ml mineral oil) was placed in the cell and immersed to the bath. After the cell was flushed three times with the experimental gas to remove residual gas and

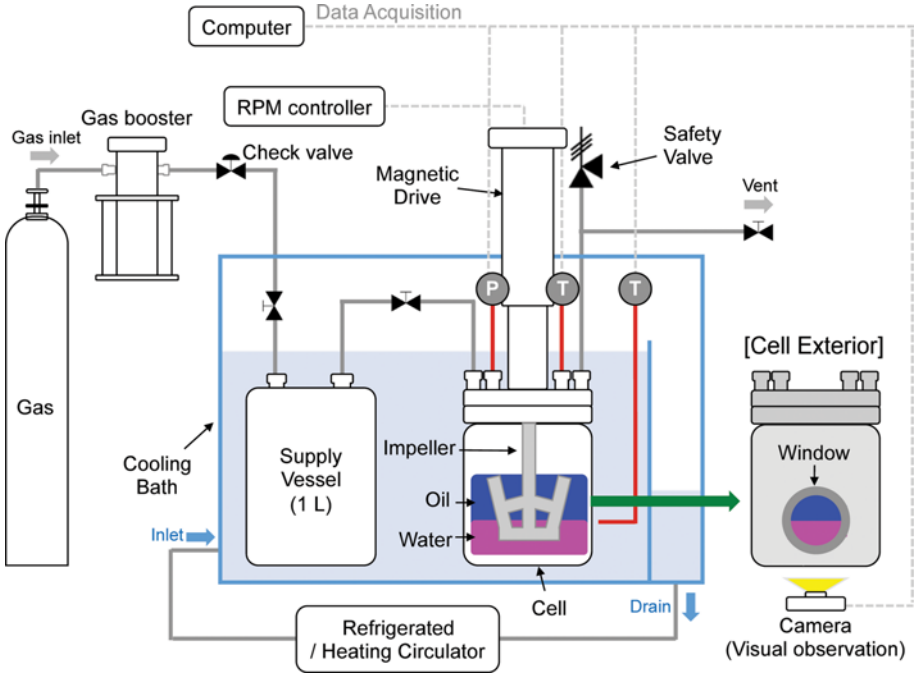

Fig. 2. Experimental apparatus used for measurements to quantify the risk for hydrate formation.

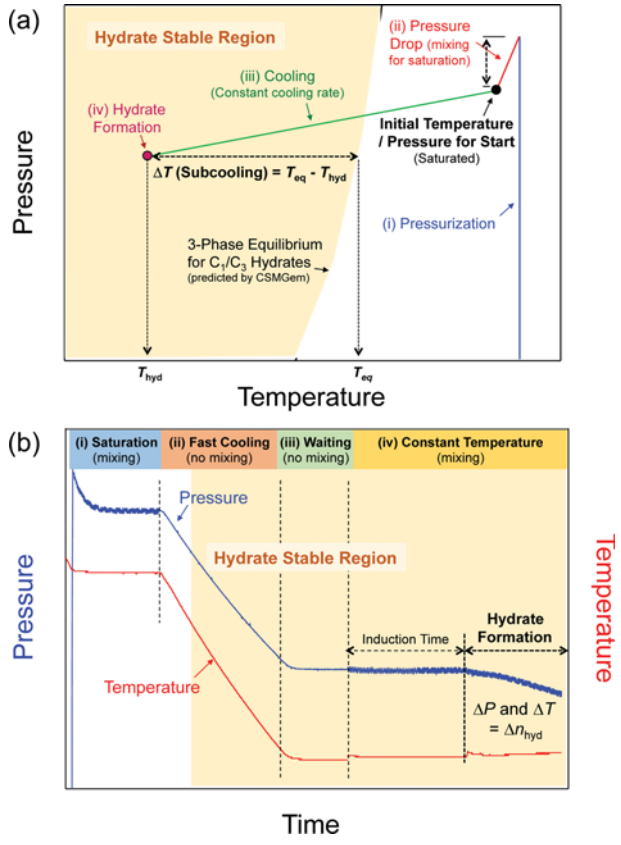

Fig. 3. Experimental procedures for quantifying the risk of hydrate formation: (a) schematic of the subcooling measurements under constant cooling rate, and (b) schematic of the measurement of hydrates formation amount at constant temperature and pressure conditions.

impurities, (i) the system (supply vessel and pressure cell) was pressurized by a gas booster, and subsequently, (ii) the liquid saturated with mixing at 300 rpm in the closed system. The system was then (iii) cooled to 277.15 K (subsea temperature) at a constant cooling rate (4 K/hr or 6 K/hr) with continuous mixing until hydrate formed (detected via temperature increase, pressure drop and visual observation), at which point the (iv) subcooling was recorded. The subcooling (ΔT) is determined by the difference between the temperature hydrates formed (T_{hyd}) and the phase equilibrium temperature (T_{eq}) predicted by CSMGem at the experimental pressure hydrates formed in Fig. 3(a). From these results, the survival curves are generated, showing there is a minimum subcooling required before hydrate can form.

In separate experiments, as shown in Fig. 3(b), we measured the initial hydrate formation rates up to 20 minutes from the time hydrates first formed with different set of temperature and pressure conditions. The initial procedure was similar to that in the subcooling measurements. After (i) pressurization and saturation in a closed system, (ii) the system temperature was quickly cooled to the target temperature without mixing, which was done to ensure that no hydrate formed during the cooling stage. The system was then allowed to (iii) reach equilibrium for some time, and then (iv) mixing was started to induce hydrate formation. Both the pressure drop and temperature changes were used to determine the amount of hydrate formed. These results were combined to develop a risk map for CH_4/C_3H_8 hydrate formation considering regions of low (green zone), medium (orange zone) and high probability (red zone).

RESULTS AND DISCUSSION

In all experiments, hydrate formation was determined by either temperature change resulting from exothermic reaction, pressure drop by gas molecules trapped in structure cages, or visual observation. For better visual observation, as mentioned in the experimental section, we used color dye for water (pink) and mineral oil (blue). Fig. 4 shows an example of hydrate formation observed: (a) well-dispersed mineral oil and water, (b) clear phase separation at the onset of hydrate formation, and (c) hydrates covered on the window surface. The observation in steps (a) and (b) is consistent with a previously reported study with mineral oil+water+gas [16]: dispersion before hydrate formation, and subsequently, phase separation oil and water at the hydrate formation onset (A video demonstrating the phase separation is available as part of the Supporting Information.). This behavior was observed in all experiments and the hydrate formation was also confirmed and matched with the temperature increase and pressure decrease in the system.

Table 1 and Fig. 5 show the experimental conditions performed

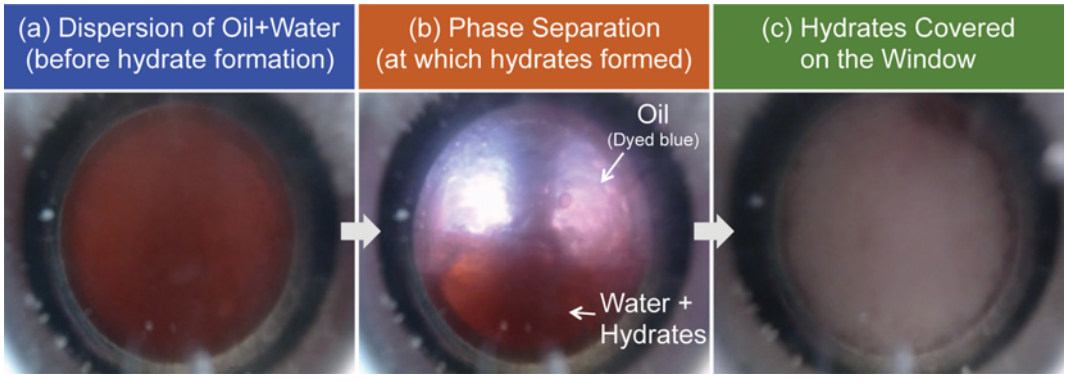

Fig. 4. Visual observation through the cell window for the state of the mixture in the cell before, during, and after hydrate formation in the mineral oil+water+gas system.

Table 1. Summary of experimental conditions performed for survival curves

Group	Total run	Initial pressure	Initial temperature	Cooling rate
A	2	6.9 MPa (1,000 psi)	298.15 K	4 K/hr
B	3	6.9 MPa (1,000 psi)	298.15 K	6 K/hr
C	12	10.3 MPa (1,500 psi)	298.15 K	4 K/hr
D	5	10.3 MPa (1,500 psi)	298.15 K	6 K/hr
E	6	13.8 MPa (2,000 psi)	298.15 K	4 K/hr
F	7	13.8 MPa (2,000 psi)	298.15 K	6 K/hr

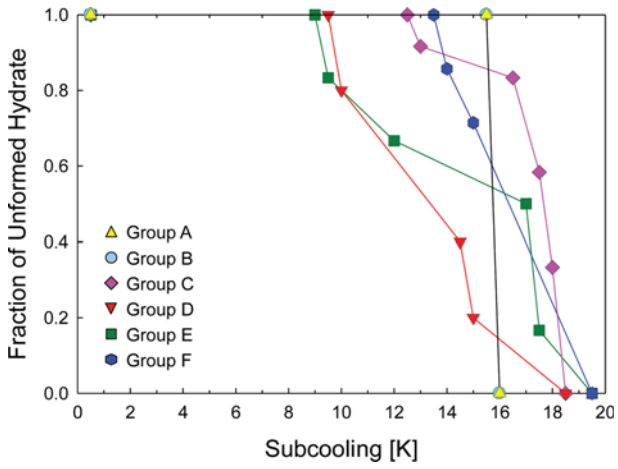

Fig. 5. Survival curves, calculated from Eq. (2), for the CH_4/C_3H_8 mixed gas hydrates measured using a linear cooling rate method for the conditions shown in Table 1 (Note that for Group A and B formed, hydrates formed at 277.15 K after a relatively long induction time of approximately 8 hours). The supporting information has details on the calculation of the survival curves.

and the survival curves, respectively, measured by the linear cooling rate method. Detailed information about the survival curves is well-introduced elsewhere [17-19]. Briefly, the survival curve is a plot of the collection of subcooling temperatures measured at the temperature hydrates formed in each individual experiment. It corresponds to the number of samples without hydrates at each instant in subcooling, measured from the subcooling the sample passes through the hydrate equilibrium temperature (T_{eq} predicted by CSMGem), divided by the total number of samples in the data set, to yield a normalized fraction of samples without hydrates based on subcooling. The fraction of formed hydrate at certain temperature interval, tK≤T<(t+0.5)K is,

$$F_{(t)}=N_t/N_{tot} \quad (1)$$

where $F_{(t)}$ is the fraction of samples with hydrate formed at a certain temperature interval tK≤T<(t+0.5)K, N_t represents the number of hydrate formation events, and N_{tot} is the total number of experiments. Consequently, the survival curve corresponds the fraction of samples without hydrate until a certain temperature interval,

$$S_{(t)}=1-\Sigma_{k=0}^{t}F_{(k)} \text{ if } F_{(t)} \text{ exists} \quad (2)$$

where $S_{(t)}$ is the survival curve, which ranges from unity at zero subcooling when all the samples are without hydrates, to zero at some high subcooling when hydrates are formed in all of the samples (The detailed process of how the survival curves are obtained from the experimental data is described in the Support Information.). All the data in Fig. 5 show that the hydrate formations occurred over a specific subcooling range from about 9 K to 16 K depending on experimental conditions. There were no samples tested that formed hydrates at a subcooling less than about 9 K. Hydrate formation is a stochastic process, but typically, as the driving force increases, the system becomes less stochastic, resulting in a narrower distribution range for the survival probability [20,21]. Based on this knowledge, we expected the range of subcooling for survival curves would be narrower at higher pressures at same cooling rate, but no clear dependence was observable in our study. Additionally, the survival curve could shift to higher subcooling with increasing cooling rate since the system spends less time at high temperatures, leading to a lower chance for nucleation. However, except for Groups E and F, we observe little dependence on the cooling rate, which is consistent with other studies in the literature [19] (Note that other studies reported in the literature are for quiescent systems, whereas we consider mixed systems.).

Several remarks need to be made for the reported survival curves: (i) the number of tests for each experimental condition in this study is limited and as such, we cannot clearly differentiate the dependence of the survival curves on temperature, pressure and cooling rate; (ii) unlike previous studies, the dynamic aspect and complexity of the chosen ternary system of oil, water and gas results in a wide variability in the initial formation of hydrates, and (iii) the specific experimental conditions in this study, such as mixing speed, liquid loading and watercut, can greatly influence the results, in particular the mixing, which promotes the contact between the phases (a much larger study would have to be done to fully address the impact of each variable). For these reasons, we focus on the minimum subcooling measured at which hydrates formed in the experiments for quantifying the risk of hydrate formation.

Fig. 6 shows the measurements of hydrate formation rate performed at various pressure and temperature conditions, and each experimental condition is represented in the inset plot in Fig. 6(b). All the measurements were repeated with fresh samples to validate the reproducibility of the results, as shown in Fig. 6(a). The hydrate conversion ratio is determined by temperature and pressure change before and after hydrate formation. The number of moles of gas consumed at given time t can be calculated with the following equation [22]:

$$(\Delta n_{gas})_t = V_{tot}\left[\left(\frac{P}{zRT}\right)_{t=0}-\left(\frac{P}{zRT}\right)_t\right] \quad (3)$$

where $(\Delta n_{gas})_t$ is the number of moles of gas consumed to form the hydrate at time t, z represents the compressibility calculated with an equation of state at temperature, T, and pressure, P, in the pressure cell at given time t, which are calculated with an equation of state, V_{tot} is the total volume of gas phase in pressure cell and tubing, which is assumed to be 1,190 mL, and R is the universal gas constant. For these calculations, we used the Peng-Robinson equation to obtain the compressibilities. Once the number of moles

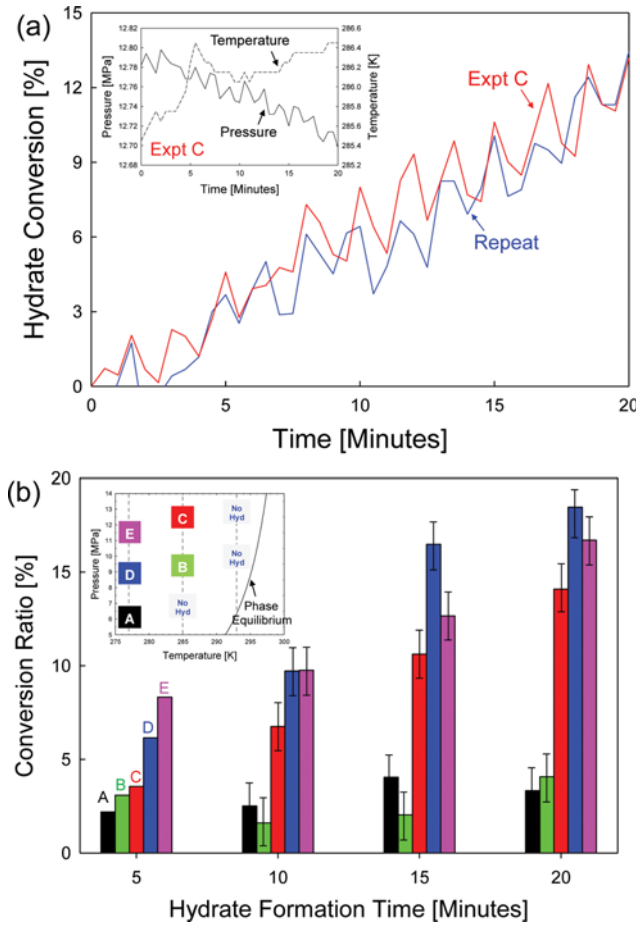

Fig. 6. Measurements of hydrate formation rates performed at constant temperature and pressure: (a) System C shown in (b) as an example of the hydrate formation rate measurements. The inset plot shows the raw pressure and temperature data in that experiment; (b) Comparison of hydrates formed in the initial 20 minutes for the conditions shown in the inset plot (Note that 'No Hyd' in inset means hydrates did not form up to 60 hours).

of gas consumed to form hydrates is determined, the amount of water consumed to form hydrates can be calculated assuming a hydration number of 6 (moles of water per moles of gas). The hydrate conversion is the fraction of water converted to hydrates. As shown in Fig. 6(a), the hydrate conversion rates fluctuate because of the fluctuations in temperature and pressure, resulting in an uncertainty of ±2.5% in the conversion ratio. Therefore, the growth rate data at 5 minutes and 10 minutes are still within the error bars. The experimental conditions are shown in the inset plot, and the conditions marked 'No Hyd' represent cases without hydrates up

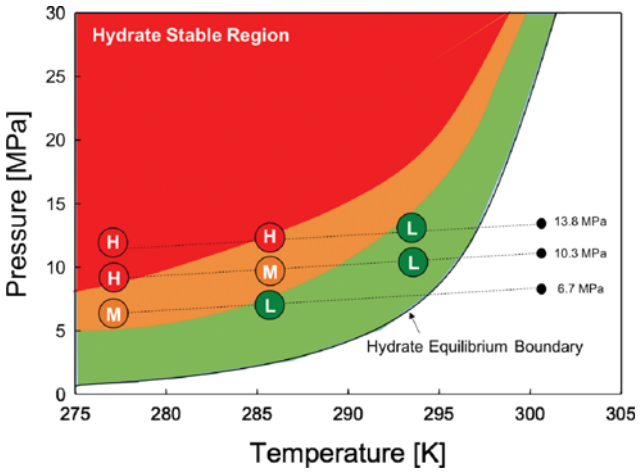

Fig. 7. A graphical risk map based on this experimental work representing H: high risk, M: medium risk, and L: low risk for hydrate formation.

to 60 hours, suggesting a low risk region for hydrate formation. For the systems A and B, which are positioned at lower pressure region, less hydrates (~5%) formed compared to other systems (C, D and E with about 13-18%) at 20 minutes, which is expected as typically more hydrates are formed under higher driving force.

Based on the results of minimum subcooling and the amount of hydrate formed for the given system considered, we propose the guidelines shown in Table 2 for quantifying the risk of hydrate formation, and consequently, the graphical risk map shown in Fig. 7. It is important to emphasize that the guidelines and risk map developed here are very specific to the set of conditions used in the study, but conceptually, this approach is applicable for any set of systems. One of the main ideas resulting from this study is that there is a "green zone" inside the hydrate stable region, and given that one can properly quantify this zone for the fluids and conditions of interest, there is an opportunity to design and operate production systems less conservatively. Each of the zones defined in Fig. 7 is strongly dependent on system and conditions, such as, gas mixture, oil type, water salinity, liquid loading, water cut, and mixing. While each of these parameters is important, a larger study would need to be done to determine their impact for significant changes in the risk assessment.

CONCLUSION

The recent approach for hydrate research in the oil and gas industry has changed from hydrate avoidance to its management. We investigated the risk of hydrate formation using measurements

Table 2. Guideline for quantifying the risk of hydrate formation performed in this study

	Subcooling	Conversion ratio
Low risk (green)	No hydrate formed	No hydrate up to 60 hours
Medium risk (orange)	8 K<ΔT<16 K	Less than 5% in 20 minutes
High risk (red)	16 K>ΔT	>5% in 20 minutes

of subcooling at which hydrates formed and the amount of hydrates at various conditions. The risk map developed has a low, medium and high probability for hydrate formation by experimentally measuring the onset of hydrates in a gas+mineral oil+water system at a given set of mixing speed, liquid loading and watercut. The measured survival curves do not show clear cooling-rate dependence or pressure dependence, but demonstrate the existence of minimum subcooling required for hydrate formation. This concept of a hydrate risk map is useful for determining the safe zones of operation and can be developed for any system.

ACKNOWLEDGEMENTS

This study was supported by a Korea Science and Engineering Foundation (KOSEF) grant funded by the Korean government and partially supported by the BK21Plus Program for advanced education of creative chemical engineers of the National Research Foundation of Korea (NRF). This work was performed at the Colorado School of Mines.

SUPPORTING INFORMATION

Additional information as noted in the text. This information is available via the Internet at http://www.springer.com/chemistry/journal/11814.

REFERENCES

1. E. Dendy Sloan Jr and Carolyn Koh, *Clathrate Hydrates of Natural Gases*, 3rd Ed., CRC Press (2007).
2. E. G. Hammerschmidt, *Ind. Eng. Chem.*, **26**, 851 (1934).
3. E. D. Sloan, C. Koh and A. K. Sum, *Natural Gas Hydrates in Flow Assurance*, Elsevier, Amsterdam (2010).
4. P. D. Dholabhai, J. S. Parent and P. R. Bishnoi, *Ind. Eng. Chem. Res.*, **35**, 819 (1996).
5. A. H. Mohammadi, W. Afzal and D. Richon, *J. Chem. Eng. Data*, **53**, 73 (2008).
6. A. Majumdar, E. Mahmoodaghdam and P. R. Bishnoi, *J. Chem. Eng. Data*, **45**, 20 (2000).
7. W. Afzal, A. H. Mohammadi and D. Richon, *J. Chem. Eng. Data*, **53**, 663 (2008).
8. W. Afzal, A. H. Mohammadi and D. Richon, *J. Chem. Eng. Data*, **52**, 2053 (2007).
9. K. Shin, J. Kim, Y.-T. Seo and S.-P. Kang, *Korean J. Chem. Eng.*, **31**, 2177 (2014).
10. A. Vysniauskas and P. R. Bishnoi, *Chem. Eng. Sci.*, **38**, 1061 (1983).
11. P. R. Bishnoi, A. K. Gupta, P. Englezos and N. Kalogerakis, *Fluid Phase Equilib.*, **53**, 97 (1989).
12. P. R. Bishnoi and V. Natarajan, *Fluid Phase Equilibr.*, **117**, 168 (1996).
13. D. Lee, Y. Lee, S. Lee and Y. Seo, *Korean J. Chem. Eng.*, **33**, 1425 (2016).
14. E. D. Sloan, *Fluid Phase Equilib.*, **228**-**229**, 67 (2005).
15. K. Kinnari, J. Hundseid, X. Li and K. M. Askvik, *J. Chem. Eng. Data*, **60**, 437 (2015).
16. E. O. Straume, C. Kakitani, D. Merino-Garcia, R. E. M. Morales and A. K. Sum, *Chem. Eng. Sci.*, **155**, 111 (2016).
17. N. Maeda, D. Wells, N. C. Becker, P. G. Hartley, P. W. Wilson, A. D. J. Haymet and K. A. Kozielski, *Rev. Sci. Instrum.*, **82**, 065109 (2011).
18. N. Maeda, D. Wells, P. G. Hartley and K. A. Kozielski, *Energy Fuels*, **26**, 1820 (2012).
19. N. Maeda, *Fluid Phase Equilib.*, **413**, 142 (2016).
20. P. W. Wilson, A. F. Heneghan and A. D. J. Haymet, *Cryobiology*, **46**, 88 (2003).
21. P. W. Wilson, D. Lester and A. D. J. Haymet, *Chem. Eng. Sci.*, **60**, 2937 (2005).
22. P. Linga, R. Kumar and P. Englezos, *Chem. Eng. Sci.*, **62**, 4268 (2007).